Fluidelastic modeling of a weathercock stabilization in a uniform flow

Ariane Gayout, Ármann Gylfason, Nicolas Plihon, Mickaël Bourgoin

Fluidelastic modelling of a weathercock stabilization in a uniform flow

Ariane Gayout[a], Ármann Gylfason[b], Nicolas Plihon[a], Mickaël Bourgoin[a]

[a] *ENSL, CNRS, Laboratoire de physique, Lyon, F-69342, France*
[b] *School of Science and Engineering, Reykjavik University, Menntavegur 1, 101, Iceland*

Abstract

The relaxation dynamics of a weathercock free-to-rotate, in the presence of a uniform flow, as it aligns with the flow direction, is investigated experimentally in a wind-tunnel. The dynamics is observed to conveniently follow a damped harmonic oscillator behavior. At first order, the frequency is set by the aerodynamic coefficients. We show that a quasi static approach fails to precisely describe the relaxation dynamics and that non-stationary corrections are required to model the dynamics. A first strategy is to introduce added mass, added stiffness and added damping to the quasi-static approximation, following what is usually done in the context of vortex-induced vibrations. A second strategy is to introduce empirical corrections, whose scaling is obtained from the analysis of the experimental data. Finally, these two strategies are compared and we discuss the physical interpretations of the non-stationary corrections.

Keywords: Time domain analysis, Aerodynamics
PACS: 47.85.Gj,
2000 MSC: 74F10, 70K25

1. Introduction

Flows and wind in particular have the particularity of bringing objects to life, by breathing movement onto them. A good example for this is how wind makes buildings sing [1] and leaves whistle [2, 3] in the audible spectrum, also known as wind-induced vibrations.

Flow induced oscillations can eventually lead to fluid-structure instabilities, with strong amplification of the oscillation amplitude. The collapse of

the Tacoma bridge in 1940 is an emblematic example. Depending on the oscillation frequency of the object relative to the characteristic aerodynamic frequency of the surrounding flow, several coupling mechanisms between the object and the fluid are generally invoked to explain such instabilities, among which Vortex Induced Vibrations (VIV) and aeroelastic flutter (also called *galloping* in civil engineering). Oscillations in flows are not necessarily associated to such dramatic instabilities, and can also be observed in stable systems which are transitionaly displaced out from equilibrium. For instance, a weathercock released in cross flow conditions will for instance oscillate as its recover its stable equilibrium position, aligned with the wind.

All these situations have in common that their description in terms of aerodynamic forces may require non-stationary aerodynamic couplings to be taken into account. This means that the coupling between the oscillating object and the wind responsible for its oscillations may not be simply modeled by static drag (lift) coefficients, C_D (C_L) of the object (as typically measured for a fixed object in a steady wind stream) as the fluid-structure interactions may become intrinsically governed by non-stationary phenomena. Spring-attached cylinders or cables are common examples which may respond to frequencies close to vortex shedding and as such be sensible to vortex-induced-vibrations (VIV). So is the oscillating weathercock. Usual non-stationary corrections include for instance added-mass effects, added damping, etc. [4, 5], or can be accounted for with modified aerodynamic coefficients.

The necessity of these corrections naturally depends on the frequency f of the oscillations of the object compared to the typical aerodynamic frequencies associated to vortex shedding f_{vs}: a quasi-static situation, where static drag (lift) coefficient apply is expected to be recovered when $f \ll f_{\text{vs}}$, as then the instantaneous aerodynamic loads can be effectively averaged over several vortex shedding periods without smoothing the slower oscillatory dynamics.

The concept of quasi-static *versus* non-stationary aerodynamic coupling is therefore crucial to the modelling of such wind-induced oscillations. To this end, it is common to introduce the reduced velocity $\text{Ur} = \frac{1}{\text{St}} \frac{f_{\text{vs}}}{f}$ (with $\text{St} = f_{\text{vs}} D/U$ the Strouhal number, D being the typical size of the oscillating object and U the mean wind velocity) or the reduced frequency $f_r = \pi/\text{Ur}$. The quasi-static approach then becomes relevant when $\text{Ur} \gg 1$ ($\text{Ur} > 20$ in practice [6]) of equivalently when $f_r \ll 1$.

In this article, we investigate wind induced oscillations in a system which

is aerodynamically stable, but which exhibits damped oscillations in the path towards its final stable equilibrium state when initially put far from equilibrium. More specifically, we consider the dynamics of a simple free-to-rotate object, a balanced disk pendulum, subject to a uniform flow. When the pendulum is initially placed with the disk facing the wind, it experiences self-oscillations until it eventually reaches its final natural equilibrium position aligned with the wind, similar to the response of a weathercock to a cross flow. We address here the question of the dynamics of this idealised weathercock through its path to equilibrium. In particular, we investigate the relevance of a quasi-static description (based on the well-known angular dependency of the normal aerodynamic coefficient $C_N(\alpha)$ of an inclined circular disk facing a uniform flow [7]) (with α the angle of attach of the disk with respect to the mean wind) and the eventual necessity of non-stationary corrections. Note that since the weathercock is balanced, contrary to a weighted pendulum, it has no prescribed natural frequency f which can be used *a priori* to estimate the reduced velocity Ur of the system in order to know beforehand the importance of non-stationary effects. As we will see, the natural self-oscillating frequency is itself an aerodynamic response whose order of magnitude can be reasonably estimated based on the quasi-static normal drag coefficient, while the overall dynamics still requires to account for non-stationary corrections. We discuss different possible strategies for such corrections, either inspired from VIV approaches or based on empirical corrections of the static normal drag coefficient of an inclined disk.

This article is organized as follows. The experimental setup, consisting of a balanced pendulum immersed in a wind tunnel, is described in Sec. 2. Signal analysis of the measurements of the time evolution of the relaxation of the weathercock towards its equilibrium position, and of their interpretation is also detailed in Sec. 2. Non-stationary corrections are then introduced in Sec. 3. Theses corrections are compared in Sec. 4 and physical interpretations of the correction parameters are discussed in Sec. 4. Finally, Sec. 5 concludes this article.

Flows and wind in particular have the particularity of bringing objects to life, by breathing movement onto them. A good example for this is how wind makes buildings sing [1] and leaves whistle [2, 3] in the audible spectrum, also known as wind-induced vibrations. However, wind-induced vibrations are not necessarily fast and many of their frequencies fall in the infrasound spectrum.

Flow induced oscillations can eventually lead to fluid-structure instabilities, with strong amplification of the oscillation amplitude. The collapse of the Tacoma bridge in 1940 is an emblematic example. Depending on the oscillation frequency of the object relative to the characteristic aerodynamic frequency of the surrounding flow, several coupling mechanisms between the object and the fluid are generally invoked to explain such instabilities, among which Vortex Induced Vibrations (VIV) and aeroelastic flutter (also called *galloping* in civil engineering).

VIV refers to a modal coupling where an instability develops whenever the characteristic aerodynamic frequency f_{vs} associated to vortex shedding (characterized by the Strouhal number $\text{St} = f_{\text{vs}}D/U$, with D the characteristic dimension of the object and U the mean wind velocity) gets close to the natural frequency f of any structural mode of the object. In such conditions, the fluid-structure interactions are intrinsically governed by non-stationary phenomena (vortex shedding) and cannot be simply modeled based on quasi-static aerodynamic coefficients (drag and lift). Usual non-stationary corrections include for instance added-mass effects, added damping, etc. [4, 5]. Spring-attached cylinders or cables are common examples which may respond to frequencies close to vortex shedding and as such be sensible to vortex-induced-vibrations (VIV).

Flutter occurs when the motion of the body modifies the effective flow seen by the body and then the aerodynamic loads and motion of the body in return. This eventually leads to a positive aerodynamic feedback with exponentially growing oscillations. When the oscillation frequency f is smaller than f_{vs}, flutter can be modeled from simple quasi-static aerodynamic coefficients. In this case, the shape of the object relative to the wind direction is the main parameter controlling the instability onset, as it conditions the evolution of the quasi-static aerodynamic coefficients as the object moves. For

instance, for a pendular system with one-degree of freedom (say its angular position α), the system may be stable or unstable under flutter depending on the angular dependency of the drag, $C_D(\alpha)$, and lift, $C_L(\alpha)$, coefficients. Flutter can take many forms, from translational motions to higher dimensional motions, including rotational and torsional modes. Translational flutter is particularly well-documented in the literature, be it experimental, numerical or theoretical approaches [5]. Due to its importance in engineering, translational-torsional flutter has been investigated extensively in the context of bridges [8, 9, 10] or transmission lines [11, 12]. On the other hand, modeling of torsional flutter has been proposed decades ago [13, 6], despite very few experimental investigations [13, 5].

The concept of quasi-static *versus* non-stationary aerodynamic coupling is therefore crucial to the modelling of wind-induced instabilities. To this end, it is common to introduce the reduced velocity $\mathrm{Ur} = \frac{1}{\mathrm{St}}\frac{f_{\mathrm{vs}}}{f}$. For VIV instabilities $f_{\mathrm{vs}} \approx f$ and Ur is of order unity ($\mathrm{Ur} \approx 5$ for an object with $\mathrm{St} \approx 0.2$). In this case, non-stationary effects cannot be neglected. When $\mathrm{Ur} \gg 1$ ($\mathrm{Ur} > 20$ in practice [6]), a quasi-static approach becomes relevant, using for instance drag and lift coefficients as traditionally measured in wind-tunnels for static objects and steady wind conditions, averaging the effective aerodynamic loads over many vortex shedding periods. While flutter often develops as a slow instability with $\mathrm{Ur} \gg 1$ compatible with a quasi-static description, depending on the body geometry, it can also appear at moderate reduced velocities, requiring in that case more complex non-stationary modeling.

The role of quasi-static and non-stationary aerodynamic couplings in wind induced oscillations phenomena is relevant beyond the sole question of fluid structure instabilities. While research on wind-induced oscillations and in particular bridge flutter, though still active, can be traced back to the 19th century [14, 15], recent environmental considerations have for instance broadened the scope of such nature-induced vibrations to the development of new ways of energy production, though flutter- and VIV-based energy harvesters [16, 17, 18, 19].

In this article, we investigate wind induced oscillations in a system which is aerodynamically stable, but which exhibits damped oscillations in the path towards its final stable equilibrium state when initially put far from equilibrium. More specifically, we consider the dynamics of a simple free-to-rotate object, a balanced disk pendulum, subject to a uniform flow. When the

pendulum is initially placed with the disk facing the wind, it experiences self-oscillations until it eventually reaches its final natural equilibrium position aligned with the wind, similar to the response of a weathercock to a cross flow. We address here the question of the dynamics of the weathercock through its path to equilibrium. In particular, we investigate the relevance of a quasi-static description (based on the well-known angular dependency of the normal aerodynamic coefficient $C_N(\alpha)$ of an inclined circular disk facing a uniform flow [7]) and the eventual necessity of non-stationary corrections. Note that since the weathercock is balanced, contrary to a weighted pendulum, it has no prescribed natural frequency f which can be used *a priori* to estimate the reduced velocity Ur of the system in order to know beforehand the importance of non-stationary effects. As we will see, the natural self-oscillating frequency is itself an aerodynamic response whose order of magnitude can be reasonably estimated based on the quasi-static normal drag coefficient, while the overall dynamics still requires to account for non-stationary corrections, in the spirit of VIV approaches.

This article is organized as follows. The experimental setup, consisting of a balanced pendulum immersed in a wind tunnel, is described in Sec. 2. Signal analysis of the measurements of the time evolution of the relaxation of the weathercock towards its equilibrium position, and of their interpretation is also detailed in Sec. 2. Non-stationary corrections are then introduced in Sec. 3. Theses corrections are compared in Sec. 4 and physical interpretations of the correction parameters are discussed in Sec. 4. Finally, Sec. 5 concludes this article.

==========
==========
==========
==========

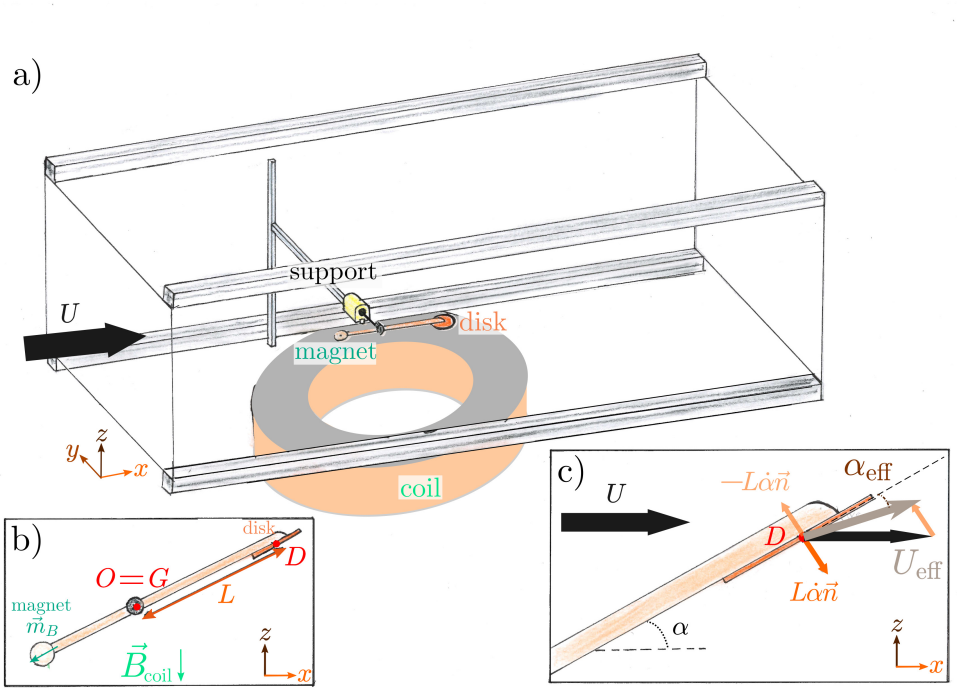

Figure 1: a)Experimental setup showing the test section of the wind-tunnel, the pendulum made of a thin disk and the coil for setting the pendulum to the vertical. b) Details on the pendulum for setting the initial position with the coil. c) Definition of the effective flow velocity U_{eff} and effective angle of attack α_{eff} acting on the moving disk.

2. Material and Methods

2.1. Experimental setup

A schematic view of the experimental setup is provided in Fig. 1. A balanced disk pendulum, acting like a weathercock, is placed in a wind tunnel. The disk pendulum consists of a thin disk of diameter d, surface area $S = \pi d^2/4$, and thickness e, made of aluminium or Vivak® and glued to a sanded saw blade of length 31 cm. The pendulum is balanced by coinciding the pivot with the center of mass. Frictionless rotation is ensured by an air bushing (OAVTB16i04 from OAV Labs) equipped with a contact-less rotary encoder that records the angular position α of the blade with minimal friction (DS-25, 17-bit digital encoder from Netzer). The typical length L between the center of mass and the center of the disk is 10 cm. In order to vary the moment of inertia of the weathercock, the blade can be weighted on the

opposite side to the disk with a thin circular magnet, aligned with the wind. In this article, we investigate the influence of the disk diameter d, the length L, the moment of inertia J on the dynamics of the weathercock relaxation. As discussed in Sec.4, the influence of these parameters is understood using a single dimensionless parameter, the reduced velocity, defined in Eq. 8. As further discussed below, for moderate wind velocities, the magnet also allows to non-intrusively impose the initial out-of-equilibrium position of the weathercock and release it on demand. Table 1 summarizes the various parameters used in the experiments presented in this article.

Diameter d_{disk} (cm)	3	4	5	6	8	9	10
Material	Al	Al	Al	Al	Al	Vivak®	Vivak®
Thickness e (mm)	0.3	0.3	0.3	0.3	0.3	0.6	0.6
Distance L (cm)	13.5	13.8	13.3	12.9	11.8	12.5	12.1
Inertia J ($\mathrm{kg\,cm^2}$)	1.34	1.57	1.66	1.89	2.24	2.57	2.90
Equivalent Ur	91.2	55.0	36.9	27.8	17.8	14.6	12.8
Equivalent k	0.034	0.057	0.085	0.11	0.18	0.22	0.25
L with magnet (cm)	17.4	17.5	17.3	16.9	16.2	16.5	16.0
J with magnet ($\mathrm{kg\,cm^2}$)	2.36	2.63	2.86	3.25	3.95	4.31	4.82
Equivalent Ur	107	63.3	42.5	31.8	20.1	16.5	14.3
Equivalent k	0.029	0.050	0.074	0.10	0.16	0.19	0.22

Table 1: Physical characteristics of the different weathercocks used in the experiment. Each disk enables for two sets of experiments, one with a magnet at the blade's opposite end and the other without. Al stands for aluminium.

The wind tunnel in which the weathercock is placed is a closed-loop wind tunnel with a square test section of $51\times51\,\mathrm{cm^2}$. The turbulence rate of the wind tunnel (defined as the ratio of the velocity standard deviation to the mean) is about 2% after the flow has been conditioned through a 6 mm honeycomb. The experiment is conducted with the weathercock in the center of the wind tunnel so that the dynamics of the weathercock is not affected by effects from the walls .

In order to carry a statistically significant characterization of the return to equilibrium of the weathercock, several realizations are repeated for each set of weathercock parameters (according to table 1) and for different mean wind velocities.

The exact same protocol is followed for all these experimental realization. First, the weathercock is set at the vertical ($\alpha = 90°$). This is achieved either

using the magnet and a coil placed below the test section of the wind tunnel (see Fig. 1 or manually using a stick. Then, the flow velocity is increased to its desired test value. The weathercock is finally released (by turning off the magnetic field or removing the stick) and left free to oscillate and to reach its final equilibrium position, which by static considerations is at the horizontal. Note, that the maximum available magnetic torque limits the magnetic release to low wind velocities (typically $U < 2\,\mathrm{m\,s^{-1}}$ for the 6 cm disk). This protocol is then repeated for about 10 times for around 8 to 14 values of U for each of the 14 weathercock configurations, leading to 751 independent realizations of the relaxation dynamics, which are analyzed in the following.

A typical time series obtained following the above-detailed protocol is shown in Fig. 2 a). This signal shows that the weathercock dynamics resembles that of a damped harmonic oscillator, sinusoidal oscillations modulated by an exponential attenuation as evidenced in Fig. 2 b). This signal can be parameterized by two characteristic times, its period $T = 2\pi/\omega$ and its attenuation time $\tau = 2/\beta$, with ω the pulsation of oscillation and β the damping coefficient. The weathercock dynamics could then be described by a simple damped harmonic oscillator equation:

$$\ddot{\alpha} + \beta\dot{\alpha} + \omega^2\alpha = 0 \tag{1}$$

This is not trivial, as the overall aerodynamic forces acting on the weathercock have complex angular dependencies, as illustrated in Fig.2 c) which represents the normal static drag coefficient $C_{N_{\mathrm{st}}}(\alpha)$ of a fixed inclined disk as a function of the angle of attack [7]. We show in the next sub-section that the damped harmonic oscillator behavior is qualitatively expected in a quasi-static description of the aerodynamics of the weathercock in the limit of small oscillations (more precisely in the range of linearity of $C_{N_{\mathrm{st}}}(\alpha)$, *i.e.* for $\alpha \in [-40°; 40°]$). In section 3 we will show however that a quantitative description requires non-stationary aerodynamic effects to be accurately accounted for.

2.2. Quasi-static momentum equation

In the absence of any weight and any external forcing other than the aerodynamic forces on the disk, the momentum equation governing the weathercock dynamics can be written as:

$$J\ddot{\alpha} = \Gamma_{aero}(t, \alpha, \dot{\alpha}) \tag{2}$$

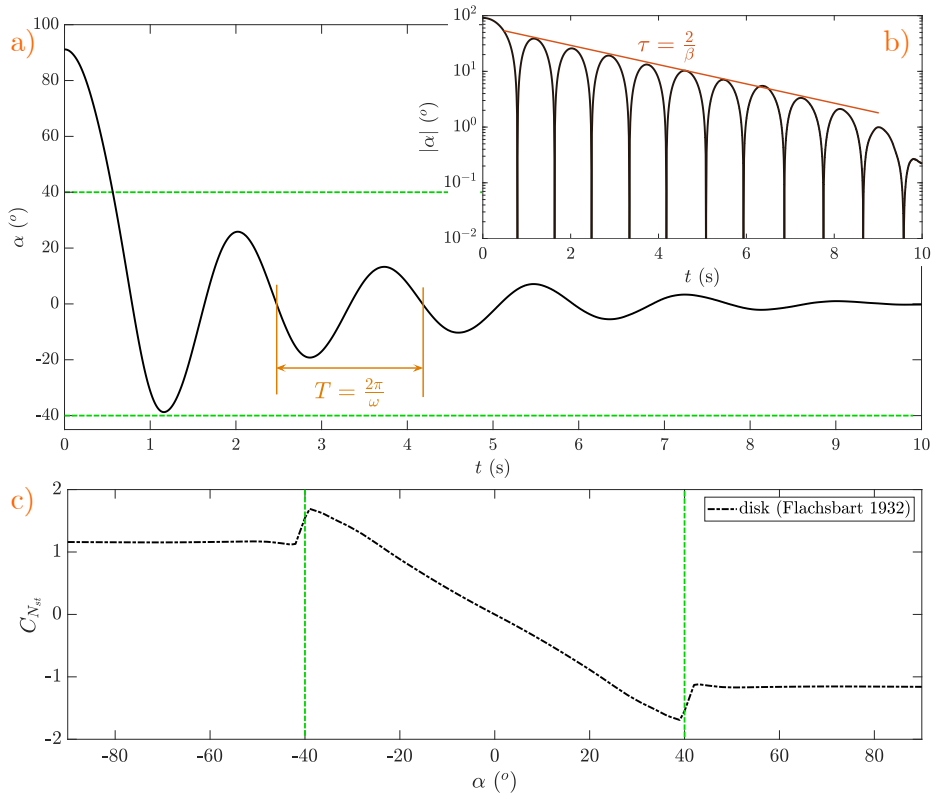

Figure 2: a) Example of an experimental signal: the pendulum is set to the vertical and left to oscillate ($d_{disk} = 4\,\mathrm{cm}$, $J = 2.63\,\mathrm{kg\,cm^2}$, and $U = 3\,\mathrm{m\,s^{-1}}$). b) Semi-log presentation of the signal amplitude over time. A pulsation ω can be defined from the period T of oscillation and a damping coefficient β can be extracted from the exponential decrease of amplitude of characteristic time τ. c) Static C_N coefficient for a disk [7], stall is represented by the dashed green lines.

with Γ_{aero} the instantaneous aerodynamic torque. Note that in a fully non-stationary situation the dependency of aerodynamic quantities as Γ_{aero} may depend on higher order temporal derivatives of the angular dynamics $\alpha(t)$ (added-mass effects, further discussed in the sequel, involve for instance acceleration dependent corrections). For the simplicity of notations we shall however only write $f(t, \alpha, \dot{\alpha})$ when referring to any instantaneous quantity f eventually subject to non-stationary aerodynamic effects.

In the range of Reynolds numbers Re investigated here (i.e. between 10^3 and 10^4, based on the mean wind velocity and the disk diameter, the aerodynamic coefficients are Re-independent. It is convenient to introduce

the normal aerodynamic coefficient C_N as $C_N = -C_L \sin(\alpha) + C_D \cos(\alpha)$, with C_L and C_D being respectively the lift and drag coefficients. A standard expression for Γ_{aero} based on dimensional analysis then reads $\Gamma_{aero}(\alpha(t), t) = \frac{1}{2}\rho S U^2 L C_N(\alpha(t), t)$, with ρ the air density, and the notation $\alpha(t)$ refers to non stationary mechanisms depending upon α, $\dot{\alpha}$ and $\ddot{\alpha}$. We stress here that the flow velocity and the angle of attack need to be corrected to account for the actual relative velocity between the disk and the mean stream [20], resulting in an effective flow velocity U_{eff} and an effective angle of attack α_{eff} (see Fig. 1.c) :

$$\left\{ \begin{array}{rcl} U_{\text{eff}}^2 & = & U^2 + 2LU\dot{\alpha}\sin(\alpha) + L^2\dot{\alpha}^2 \\ \alpha_{\text{eff}} & = & \alpha + \arctan\left(\dfrac{L\dot{\alpha}\cos(\alpha)}{U + L\dot{\alpha}\sin(\alpha)}\right) \end{array} \right. \tag{3}$$

A first approximation for the expression of normal drag coefficient $C_N(\alpha_{\text{eff}}(t), t)$ is to use its static value $C_{N_{st}}(\alpha_{\text{eff}})$, which is tabulated in the literature for static inclined disks [7], and is displayed in Fig. 2 c). The quasi-static weathercock dynamics then follows the equation :

$$J\ddot{\alpha} = \frac{1}{2}\rho S L U_{\text{eff}}^2 C_{N_{st}}(\alpha_{\text{eff}}(t)) \tag{4}$$

A Taylor expansion in α around the equilibrium position $\alpha = 0°$ (considering the expressions for α_{eff} and U_{eff} in eq. (3)), then leads to a damped harmonic oscillator equation,

$$\ddot{\alpha} + \beta_{st}\dot{\alpha} + \omega_{st}^2\alpha = O(\alpha^3) \tag{5}$$

reminding of Eq.1 with

$$\left\{ \begin{array}{rcl} \omega_{st}^2 & = & \dfrac{\rho S L U^2}{2J} \left.\dfrac{\mathrm{d}C_{N_{st}}}{\mathrm{d}\alpha}\right|_0 \\ \\ \beta_{st} & = & \dfrac{\rho S L^2 U}{2J} \left.\dfrac{\mathrm{d}C_{N_{st}}}{\mathrm{d}\alpha}\right|_0 = \dfrac{L}{U}\omega_{st}^2 \end{array} \right. \tag{6}$$

We note here that the pulsation of the quasi-static regime is given by the slope of the C_N coefficient at the origin. We expect the expansion around $\alpha = 0°$ to hold over the entire linear regime of $C_{N_{st}}$, *i.e.* up to the stall angle ($\alpha \sim 40°$, see fig. 2a), which means that this approximation should hold for the observed relaxation dynamics after the first minimum for the

signal shown in Fig. 2 (i.e. for $t > 1.2\,\mathrm{s}$). We also stress that the quasi-static modeling does not take into account the unsteadiness behavior due to vortex shedding and is thus expected to fail for the lowest values of the reduced velocity, as developed in the next section.

3. Results

Following the previous considerations, it is tempting to compare the measured weathercock relaxation dynamics towards equilibrium to the quasi-static damped oscillator dynamics associated to Eq. (5). Figure 3 shows the experimental values for ω^2 and β (computed by fitting the experimental signals as a damped harmonic oscillator dynamics) as functions of their estimations using the static coefficient approximation ω_{st}^2 and β_{st} (Eq. (6)). It can be seen that, for the range of explored parameters, both the the oscillating pulsation ω and the damping coefficient β are linearly related to the quasi-static predictions. The quasi-static damping coefficient β_{st} slightly underestimate the actual damping coefficient β, while the quasi-static estimate of the the pulsation ω_{st} systematically overestimate the actual pulsation ω. This suggests that, although the quasi-static approximations ω_{st} and β_{st} give the correct order of magnitude for the oscillating frequency and damping, corrections to the quasi-static model are still required. The quasi-static values for the oscillating frequency and the damping coefficient can therefore be considered as a reasonable first order approximation, from which quantitative corrections are to be derived in the frame of a refined modelling of the weathercock dynamics. In the following, we propose two ways of recovering the experimental dynamics by extending the quasi-static dynamics given by Eq. (4), first in the context of a VIV-inspired expansion, second by introducing an empirically determined dynamical normal drag coefficient $C_{N_{in}}$. According to Eq. (2), the corrections are expected to depend not only on the angular position α, but explicitly upon the time t and/or the higher time derivatives of $\alpha(t)$ (angular velocity and acceleration). In the following, we introduce such corrections that can be computed *a priori*, and we show that they only depend upon the reduced velocity Ur or the flow velocity U.

3.1. VIV-inspired time domain correction

We propose in this section a refinement of the quasi-static model accounting for possible non-stationary corrections that would be responsible for the deviations observed for the weathercock dynamics, in particular regarding

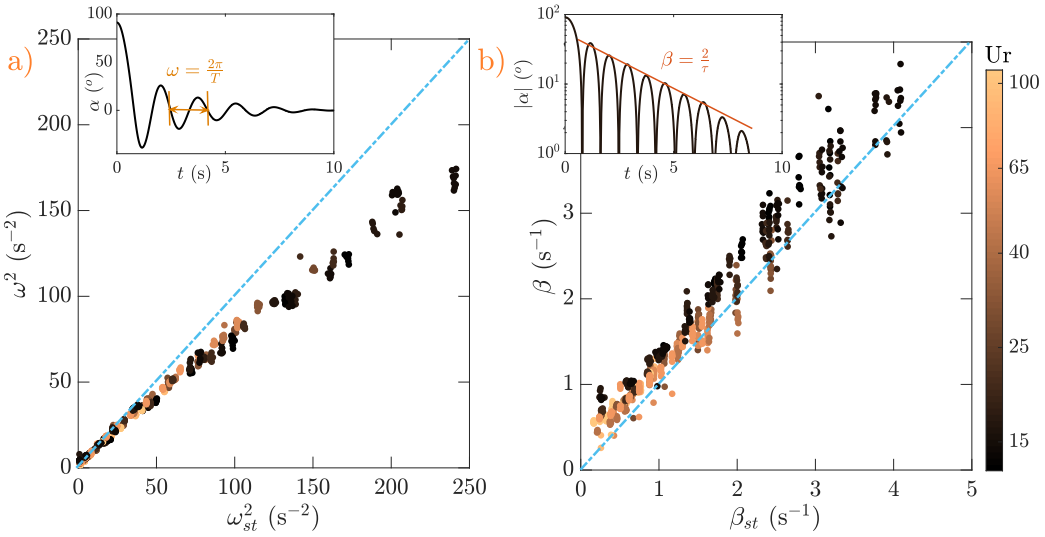

Figure 3: a) Experimental measured pulsation ω^2 with respect to the static estimated pulsation ω_{st}^2. b) Experimental measured damping coefficient β with respect to the static estimated damping β_{st}. Dash-dotted lines represent identity and the color codes for the Ur parameter of each experiment on both graphs.

the expected oscillation frequency. When such frequency shifts are observed in unsteady aerodynamics, a common theoretical approach is the addition of stiffness and mass to the dynamics equation, thus taking into account the effective global impact of vortex shedding on the free dynamics. We note that for a rotating system as the one investigated here, the equivalent of an added mass would correspond to an added moment of inertia.

This approach, mostly used in vortex-induced vibration (VIV) theory, assumes that the behavioral dynamics depends on the ratio between the vortex shedding frequency and the frequency of natural oscillation of the system. Non-stationary aerodynamic corrections are expected to be dominant when natural oscillations are rapid or comparable to vortex shedding, while a quasi-static approach should hold for slow oscillations. As already stated in Sec. 1, this competition between natural oscillations and vortex shedding is usually quantified by the reduced velocity Ur, a characteristic dimensionless number which characterizes the unsteadiness of the aerodynamic couplings:

$$\mathrm{Ur} \equiv \frac{1}{\mathrm{St}} \frac{f_{vs}}{f} = \frac{U}{df}, \tag{7}$$

where f_{vs} is the vortex shedding frequency, f the natural oscillation frequency

of the structure in the wind and $\mathrm{St} = df_{vs}/U$ the Strouhal number.

In the present situation, as the weathercock is perfectly balanced, it has no structural natural oscillation frequency associated to its rotational dynamics (contrary to a weighted pendulum for instance). The linear relation between ω and ω_{st} shows indeed that the oscillation frequency has an aerodynamic origin, whose order of magnitude and trends are reasonably captured by the quasi-static Eq. (6). In the present case, the reduced velocity is therefore defined using the quasi-static oscillating frequency: $f = f_{st} \equiv \omega_{st}/2\pi$. This leads to the following expression for Ur:

$$\mathrm{Ur} = \frac{1}{\mathrm{St}}\frac{f_{vs}}{f} = \frac{U}{d}\frac{2\pi}{\sqrt{\frac{1}{2}\frac{\rho S U^2 L}{J}\left.\frac{\mathrm{d}C_N}{\mathrm{d}\alpha}\right|_0}} = \frac{4}{d^2}\sqrt{\frac{2\pi J}{\rho L\left.\frac{\mathrm{d}C_N}{\mathrm{d}\alpha}\right|_0}}. \tag{8}$$

Remarkably, Ur is found to be independent of the flow velocity U, linked to the fact that the natural oscillations of the balanced weathercock are self-induced by aerodynamic couplings. As such, Ur is varied in the experiments by the modifications of parameters d, J and L of the weathercock. The range of explored Ur in this study spans from 14 to 120 (see Table1). We note that this broad range of accessible values of reduced velocity confirms that the observed oscillations of the weathercock are not primarily driven by vortex shedding, what would lead to values of $\mathrm{Ur} = \mathcal{O}(\mathrm{St}^{-1}) \simeq 10$ (since the Strouhal number for flat disks as investigated here is of order 10^{-1} [21]). Vortex shedding is however expected to contribute to the observed deviations of the weathercock dynamics when compared to the quasi-static description. Modeling its contribution to the weathercock dynamics is the goal of this subsection.

In vortex-induced vibration models, added mass, stiffness and damping are appended to the system dynamics equation in the simplest possible way, as additive linear corrections to the quasi-static equation Eq. (5), which becomes:

$$(1+m)\ddot{\alpha} + (\beta_{st} + \gamma U)\dot{\alpha} + (\omega_{st}^2 + k)\alpha = 0 \tag{9}$$

with m the added mass (added moment of inertia in the present case), γU the added damping and k the added stiffness, all normalized by the moment of inertia J. It follows that in the context of this refined model, the corrected predictions for the oscillation pulsation and damping coefficient are:

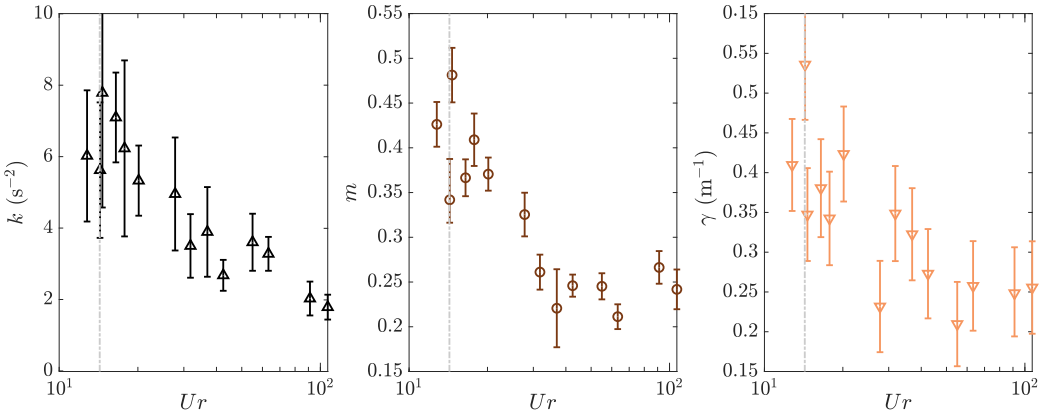

Figure 4: Added stiffness k, mass m and damping γ obtained for each Ur parameter in the experiments. Dash-dotted line represents 1/St with St $\simeq 0.07$.

$$\begin{cases} \omega_{\text{viv}}^2 &= \dfrac{\omega_{\text{st}}^2 + k}{1+m} \\ \beta_{\text{viv}} &= \dfrac{\beta_{\text{st}} + \gamma U}{1+m} \end{cases} \tag{10}$$

Figure 4 shows the three added parameters (k, m and γ) as functions of the reduced velocity Ur (the parameters are obtained by fitting the measured oscillation pulsation and damping with expressions (10)). The three of them exhibit the same overall trend with a peak around Ur $\simeq 15$ followed by a rapid decrease as Ur increases. The peak is attained for a value of reduced velocity of the order of Ur $\sim \text{St}^{-1} \simeq 15$ (St$\simeq 0.07$ is the value reported in the literature for transverse vortex shedding for a disk [22] ; the vertical dashed line in Fig. 4 indicates St^{-1}). Such a "diverging" behavior around UrSt ~ 1 (*i.e.* $f = f_{vs}$) is expected in VIV systems, as it corresponds to situations for which the object oscillations and vortex shedding couple together due to the similarity of frequencies, leading to lock-in synchronicity between vortex shedding and natural oscillations.

Overall, the trends observed in Fig. 4 are in agreement with the intuitive expectation that non-stationary corrections become preponderant when the oscillation frequency approaches that of vortex shedding. As expected these corrections then rapidly decrease as the reduced velocity increases (*i.e.* as the oscillation frequency becomes significantly smaller than vortex shed-

ding frequency). The available data does not allow to be fully conclusive on whether the corrective parameters would decrease to zero as Ur keeps increasing or would tend to a finite, non-vanishing, asymptotic value. Hence, the quasi-static approximation is approached but not fully recovered even for Ur ~ 100, while it is expected to hold in the the limit Ur $\to \infty$. We cannot rule out the blade to be at the origin of these non-vanishing values of the added coefficients for Ur ~ 100, especially since the largest values of Ur were probed using the smallest 3-cm diameter disk.

Another observation is that the maximum value of the added mass is close to 0.5, which reminds of the added mass coefficient found in particle-laden flows for a sphere immersed in fluid. A possible interpretation for this value would thus be that at synchronization of oscillations with vortex shedding, the disk and its wake behave as an effective "sphere" of fluid that does only detach at specific moments in the oscillation cycle.

3.2. Empirically corrected C_N coefficient approach

We now investigate an empirical model, which, contrary to the previous approach, does not assume *a priori* a damped-harmonic oscillator behavior. It is indeed possible to empirically retrieve an instantaneous normal drag coefficient $C_N(\alpha_{\text{eff}}(t), t)$ using Eq. 4 and the experimental measurement of the angular dynamics of the weathercock.

The experimental instantaneous C_N coefficient is compared to its static equivalent $C_{N_{st}}$ computed from reported measurements for a fixed disk [7] (dashed blue line) in Fig. 5.a), as a function of the effective angle of attack α_{eff}. The color codes the flow velocity U from $3.8\,\text{m}\,\text{s}^{-1}$ (lighter color) to $8\,\text{m}\,\text{s}^{-1}$ (darker color) with steps of $0.7\,\text{m}\,\text{s}^{-1}$. Interestingly, the instantaneous $C_{N_{in}}$ recovers (after the first oscillation) a simple linear angular dependency, in the range $\alpha_{\text{eff}} \in [-40°; 40°]$, reminiscent of the linear region for the static coefficient $C_{N_{st}}$. We observe however that the slope of the linear region is strongly dependent on experimental conditions: it is consistently close to the static case for the lowest tested wind velocity U, but then systematically decreases when U is increased. This dependency on U is less pronounced on the initial oscillation starting at $\alpha = 90°$, although the global behavior on this part of C_N strongly deviates from the static behavior. This initial phase, which is strongly affected by the effects of stall, is out of the scope of the present study and shall be further explored in the future.

Another interesting observation is that the evolution of the ratio of the slope of the instantaneous $C_{N_{in}}(\alpha_{eff})$ coefficient to the slope of the static

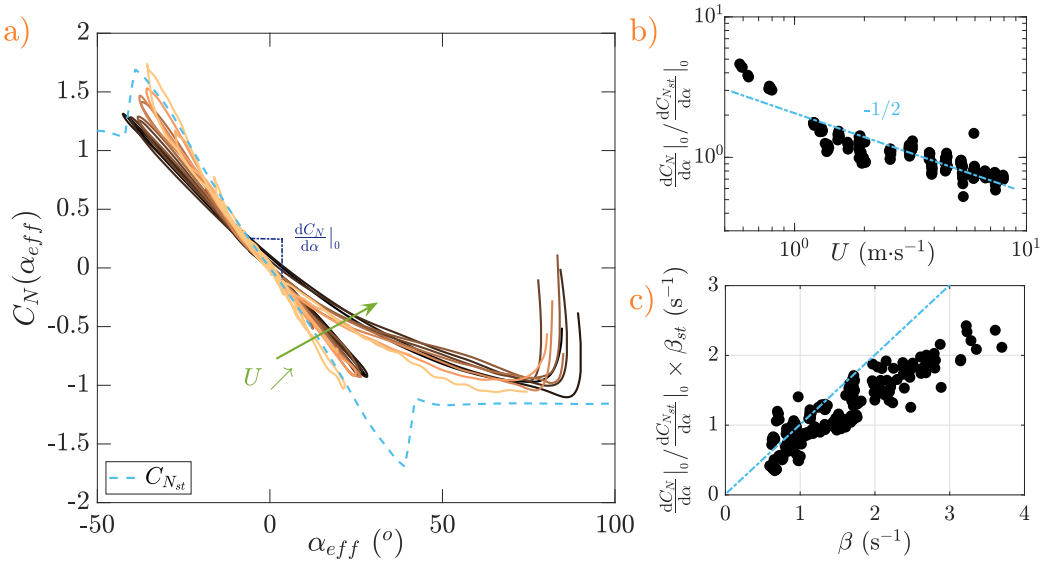

Figure 5: a) Dynamic (solid lines) vs static (dashed line) C_N coefficients as function of the angular position α_{eff} given by Eq. 3 for various flow velocities U, which color codes as follows: the lighter the color, the smaller U. b) Ratio between the slope of the dynamic $C_{N_{in}}$ coefficient and the static coefficient $C_{N_{st}}$ with respect to flow velocity. c) Damping coefficient β_{em}, estimated from the empirical correction on the $C_{N_{st}}$ coefficient, compared to the experimental damping β.

$C_{N_{st}}(\alpha_{eff})$ coefficient exhibits a $U^{-1/2}$ power as a function of the flow velocity U (see Fig. 5.b).

Overall, these observations suggest that, in the range of interest ($\alpha_{eff} \in [-40°; 40°]$, i.e. after the first oscillation) a simple empirical correction to the quasi-static approach can be formulated using an effective instantaneous normal drag coefficient, with a linear angular dependency whose slope is related to the static case as:

$$\left.\frac{\mathrm{d}C_{N_{in}}}{\mathrm{d}\alpha}\right|_0 = \left(\frac{U^*}{U}\right)^{1/2} \left.\frac{\mathrm{d}C_{N_{st}}}{\mathrm{d}\alpha}\right|_0, \tag{11}$$

where the coefficient $U^* = U \left(\left.\frac{\mathrm{d}C_{N_{in}}}{\mathrm{d}\alpha}\right|_0 \Big/ \left.\frac{\mathrm{d}C_{N_{st}}}{\mathrm{d}\alpha}\right|_0 \right)^2 \simeq 3.7\,\mathrm{m\,s^{-1}}$ is obtained by the fit shown in Fig. 5b). In order to explore the capacity of this corrected drag coefficient model to capture the weathercock dynamics, we have solved Eq. (4) using this corrected drag coefficient. The corrected model nicely reproduces the damped harmonic oscillator dynamics observed in the experiment, with an almost perfect match for the oscillation frequency and a reasonable match of the damping coefficient. To better understand the effect of the corrected drag coefficient, we can consider the same linearization of Eq. (4) previously introduced for the quasi-static approximation and leading to Eq. (5), but using relation (11) as normal drag coefficient. The additional $U^{1/2}$ factor in C_N modifies the linearized dynamics of Eq. (5) which now reads:

$$\ddot{\alpha} + \beta_{em}\dot{\alpha} + \omega_{em}^2\alpha = O(\alpha^3), \tag{12}$$

where ω_{em} and β_{em} are respectively the empirically predicted oscillation pulsation and damping:

$$\begin{cases} \omega_{em}^2 &= \omega_{\mathrm{st}}^2 \left.\frac{\mathrm{d}C_{N_{in}}}{\mathrm{d}\alpha}\right|_0 \Big/ \left.\frac{\mathrm{d}C_{N_{st}}}{\mathrm{d}\alpha}\right|_0 \\ \beta_{em} &= \beta_{\mathrm{st}} \left.\frac{\mathrm{d}C_{N_{in}}}{\mathrm{d}\alpha}\right|_0 \Big/ \left.\frac{\mathrm{d}C_{N_{st}}}{\mathrm{d}\alpha}\right|_0 \end{cases} \tag{13}$$

The damping coefficient β_{em} is plotted against the experimental damping coefficient in Fig. 5.c), from which it is clear that an additional damping term is necessary to correctly describe the observed experimental dynamics. Remarkably, the strength of this additional damping is close to the added

damping γU from the previous model (not shown here). While its origin is not clear, the strength of this additional damping as a function of d_{disk} is discussed further in section 4.

4. Discussion

In this section, we briefly discuss possible physical interpretations of some of the additional parameters introduced to improve the non-stationary modelling of the weathercock dynamics and then compare the performances of the different modelling strategies (quasi-static, VIV-inspired, empirical drag coefficient).

4.1. Physical interpretation of the modelling parameters

Let us first discuss the terms added in the model introduced in Sec. 3.1. In particular, the added mass (or added inertia) can be interpreted, like in particle-laden flows and VIV, as the mass of fluid displaced and dragged by the disk during its motion. We can therefore compute the diameter d_{air} of an equivalent air sphere around the disk centered at the center of the disk and of moment of inertia mJ:

$$d_{air}^3 \left(L^2 + \frac{d_{air}^2}{10} \right) = \frac{6mJ}{\pi\rho} \tag{14}$$

As shown in Fig. 6.a), this diameter d_{air} is almost linear in the diameter of the disk d_{disk} (with a plateau at the smaller values probably due to the influence of the rod holding the disk), consistent with the idea that larger disks drag a proportionally larger equivalent sphere of air.

A phenomenological interpretation of the added stiffness is much more difficult to conduct. However, it could be linked to the dynamics of the wingtip vortices as α changes sign. Indeed, when the weathercock crosses the horizontal, the upper surface becomes the lower surface and the vorticity of the wingtip vortices is expected to change sign. This could lead to a restoring spring-like torque $-k\alpha$ due to the coupling of the wingtip vortices with to the leading- and trailing-edge vortices.

Regarding the added damping in the VIV inspired model, we define a corrective term $\epsilon = \dfrac{\gamma U}{\beta_{st}}$, such that $\beta_{\text{viv}} = \beta_{\text{st}} \left(\dfrac{1}{1+m} + \epsilon \right)$. ϵ represents the correction required with respect to the quasi-static description, regardless of the added mass modification $\frac{1}{1+m}$ to the quasi-static damping. The evolution

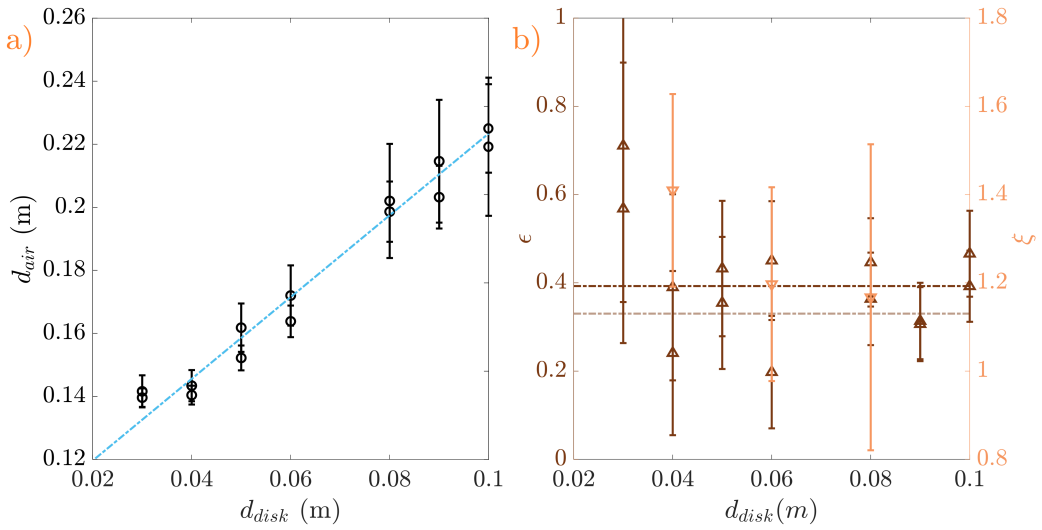

Figure 6: Evolution of the interpreted added terms d_{air} (a), ϵ (b left axis) and ξ (b right axis) as functions of the diameter of the disk d_{disk}.

of ϵ as a function of the pendulum diameter d_{disk} for each pendulum configuration is displayed in Fig. 6 b). The value for the smaller disk is close to 0.7, and despite large error-bars, ϵ tends to converge at higher d_{disk} towards a constant value ϵ_c, represented by the dash-dotted lines.
Strikingly, a good candidate for this value is $\epsilon_c = \frac{\pi}{8}$ (dark line), which can be related to the damping of unsteady aerodynamic flutter models using potential flow theory [23, 6].

Let us now discuss the empirical model presented in Sec. 3.2. As introduced previously, an additional damping to β_{em} is required to correctly describe the dynamics. It is formally equivalent to implement this additional damping directly into equation Eq. (4) as a correction on α_{eff} and U_{eff}, without changing the form of equation Eq. (4) (though for the latter correction, it would only result in a 3rd order correction, which will be neglected in the linearized dynamics considered here). It can indeed be noticed that the damping β_{st} emanates from the $L\dot{\alpha}/U$ term in Eq. (5), which is the approximation taken for the relative velocity of the counter flow in response to the pendulum movement (see Fig. 1c)). The required additional damping can thus be accounted for by a multiplicative factor $\xi = \dfrac{\beta}{\beta_{em}}$ on the $L\dot{\alpha}/U$ term,

resulting in modified effective parameters:

$$\left\{ \begin{array}{rcl} U_{\text{eff}}^{*2} & = & U^2 + 2\xi LU\dot{\alpha}\sin(\alpha) + \xi^2 L^2\dot{\alpha}^2 \\ \alpha_{\text{eff}}^{*} & = & \alpha + \arctan\left(\dfrac{\xi L\dot{\alpha}\cos(\alpha)}{U + L\xi\dot{\alpha}\sin(\alpha)}\right). \end{array} \right. \tag{15}$$

In this context, the dynamics of the weathercock now reads:

$$J\ddot{\alpha} = \frac{1}{2}\rho SLU_{\text{eff}}^{*2} C_{N_{st}}(\alpha_{\text{eff}}^{*}) \left.\frac{\mathrm{d}C_{N_{in}}}{\mathrm{d}\alpha}\right|_0 \Big/ \left.\frac{\mathrm{d}C_{N_{st}}}{\mathrm{d}\alpha}\right|_0$$

Estimated values for ξ are presented in Fig.6.b), for three different configurations as examples. Though the uncertainty on the damping and empirical correction makes it difficult to be fully conclusive on the value of ξ and its trend, an observation to be made yet is that ξ appears to be higher than 1, meaning that when the aerodynamic coefficient is pondered by a dynamical term, the air around the pendulum moves at a higher velocity than the pendulum its self. This could be explained by the fact that not only the air behind the pendulum is dragged away but the air ahead is deviated as well, and may induce an supplementary advection for the air behind.

4.2. Comparison of models

Here we aim explore the accuracy of the different modelling strategies (quasi-static, VIV-inspired, empirical C_N) in capturing the experimental behavior of the weathercock. We compare the solution of the modelling equations and the experimental signal for the same initial conditions as in the experiment ($\alpha(0) \simeq 90°$ and $\dot{\alpha}(0) \simeq 0\,°\,\mathrm{s}^{-1}$). The corresponding signals are shown in Fig. 7 a). To quantify the discrepancy between the experiment and the modeling we compute the quadratic angular error $\sqrt{\langle \Delta\alpha^2 \rangle}$ between the experimental signal and each of the models.

While the VIV-inspired model collapses almost perfectly on the experiment with $\sqrt{\langle \Delta\alpha^2 \rangle} \leq 2°$, the empirical C_N model happens to be quite wrong as $\sqrt{\langle \Delta\alpha^2 \rangle} \simeq 10°$. This is due to the lack of capacity the this model to reasonably reproduce the transient dynamics of the first oscillation, which is strongly impacted by the complex behavior of C_N when the disk passes the stall angle. The good capacity of the VIV-inspired model to reasonably capture this transient while the corrective model and coefficients (added inertia, damping and stiffness) have only been derived based on the linearized dynamics past the first oscillation, is striking. The static model exhibits a relatively

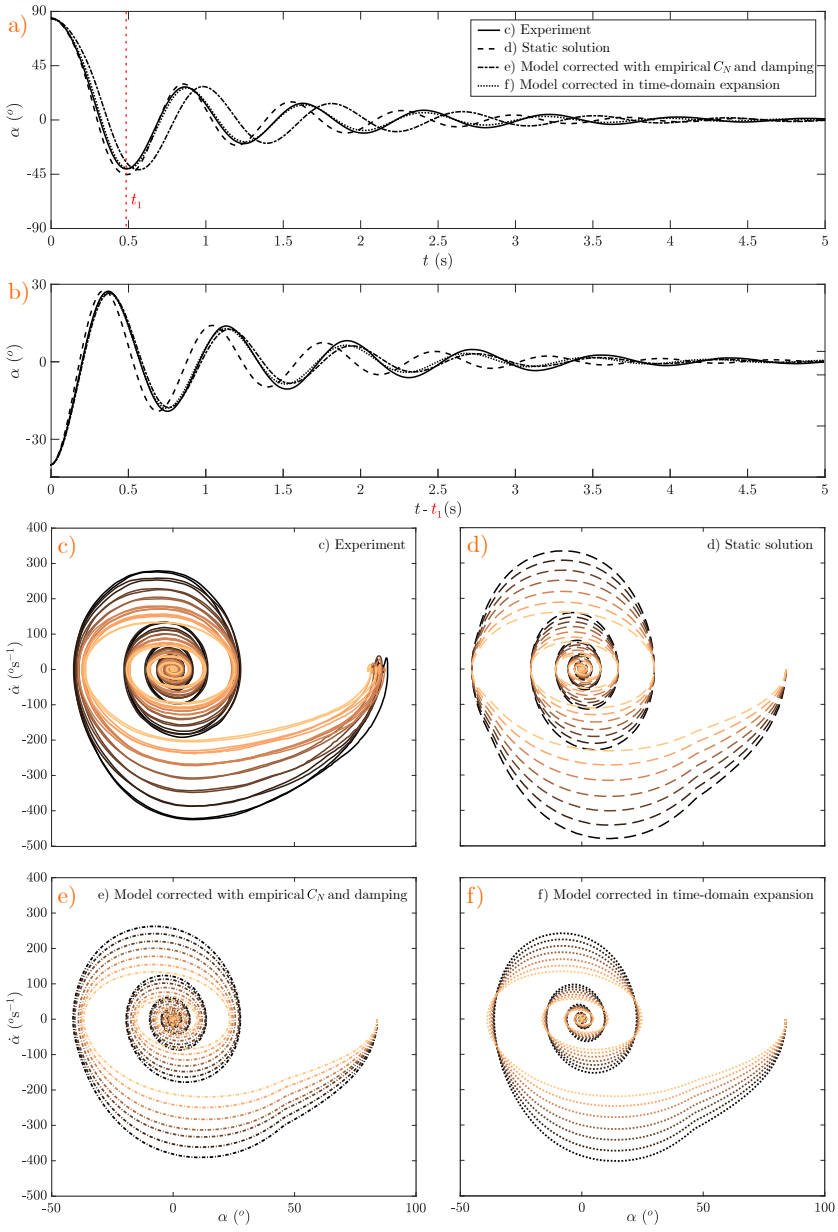

Figure 7: Comparison between the experimental signal and the models with initial conditions a) at the vertical and b) at the first minima of oscillation. Phase portraits for the experiment and models: c) experiment, d) static coefficient model, e) empirical dynamic coefficient model with added damping and f) time-domain expansion model. The color codes for the flow velocity, with the lighter being the smaller velocity. All presented curves were obtained from the 4 cm weathercock with magnet attached, similar results were obtained for the other weathercocks.

small global deviation from the experimental signal, of about $\sqrt{\langle \Delta\alpha^2 \rangle} \simeq 5^\circ$ only, despite the lack of fidelity in both frequency and damping.

In order to ignore the impact of the transient dynamics, we have considered the situations where the initial condition is taken at the first minimum of oscillation (t_1), hence already past the stall angle and in the linear part of the C_N coefficient. The corresponding signals, both experimental and from the models, are shown in Fig. 7 b) as a function of $(t-t_1)$. It can be seen that in that case, the VIV-inspired model and the empirical C_N model capture almost perfectly (with $\sqrt{\langle \Delta\alpha^2 \rangle} \simeq 1^\circ$) the relaxing dynamics of the weathercock. The quasi-static dynamics is on the contrary at odds, indicating that the moderate error noted for the previously discussed initial conditions was fortuitous.

Finally, for a deeper insight into the dynamical fidelity of the modelling we consider the phase portraits (in $(\alpha, \dot{\alpha})$ space) of the weathercock dynamics (Fig. 7.c-f). From this point of view, while all models reasonably capture the qualitative behavior of the experiment, the match seems to be greater for the empirical C_N model, especially regarding the flow velocity dependence.

Hence to conclude, for small oscillations, the two models we propose in this paper to account for non-stationary aerodynamics correctly reconstruct the dynamics of the system. However if large oscillations are observed, the VIV-inspired corrections transcribe better the behavior of stabilization, although further dedicated investigation focusing on the dynamics near stall would be required to clarify whether this is a reliable or a fortuitous observation.

5. Conclusion

We have presented two very different approaches to incorporate non-stationary effects into the static aerodynamic modeling of a relaxing weathercock made of a balanced pendulum composed of a flat disk at the end of a freely pivoting rod. Past the first oscillation, the weathercock dynamics was found to be well approximated by a damped harmonic oscillator behavior, hence characterized by its oscillation frequency and exponential damping coefficient. In the limit of small angles ($|\alpha| < 40^\circ$) this dynamics is qualitatively retrieved by a simple quasi-static model considering only the (linear) angular dependency of the static normal drag coefficient $C_{N_{\text{st}}}$ of a fixed inclined disk. This model reasonably captures the qualitative dynamics, but fails capturing the accurate values for the oscillation frequency and damping coefficient. The

deviations increase as the frequency of oscillation increases, hence suggesting that non-stationary aerodynamics effects must be considered to accurately model these situations. To do so, we have first considered a VIV-inspired approach, where effects of non-stationarity are modeled based on added moment of inertia, added damping and added stiffness. Our results show that the importance of these corrections increases when the reduced velocity Ur (which in our case does not depend on the wind-speed and is entirely defined by the weathercock geometry) decreases and approaches a value close to the inverse St^{-1} of the Strouhal number associated to transverse vortex shedding, suggesting a strong coupling between shedding and oscillations of the weathercock in such conditions. As Ur increases, the non-stationary corrections decrease, and remain finite even for Ur $\sim 10\mathrm{St}^{-1}$ hence pointing that even at high values of Ur (*i.e.* when oscillations are slow compared to vortex shedding the effective normal drag coefficient to be considered for a quasi-statically freely rotating disk may still deviate from the case of fixed disk.

As a second modelling strategy of the weathercock dynamics, we have introduced an empirically determined instantaneous normal drag coefficient. Our results suggest that, in the angular region of interest ($|\alpha| < 40°$) this instantaneous drag coefficient follows the same angular dependency as the static drag coefficient, but that a velocity dependent factor should be introduced. This factor was found to scale as ($U^{1/2}$) possibly pointing to a possible role played by skin friction effects, although future studies would be required to gain insight into this observation. The comparison of the performances of the two modelling strategies with respect to the experimentally measured weathercock dynamics shows that in the linear region ($|\alpha| < 40°$), both models very accurately reproduce the motion of the weathercock. Interestingly, the VIV-inspired model also behaves reasonably well beyond the linear domain for which it has been built, in particular when the weathercock passes by the static stall angle, a transient that the empirical C_N model fails to capture. Whether the good behavior of the VIV-inspired model in this transient is real or fortuitous would require further dedicated studies around the stall angle.

Acknowledgements

The authors acknowledge financial support of the Project IDEXLYON of the University of Lyon in the framework of the French Programme Investisse-

ments d'Avenir (ANR-16-IDEX-0005) and of the Laboratoire de Physique for the upgrade of the wind-tunnel. The authors warmly thank J. Borée, Y. Haffner and C. Sicot for stimulating discussions.

References

[1] J. Berhault, Wind noise in buildings, Wind Engineering 1 (1) (1977) 67–82.

[2] O. Fegeant, Wind-induced vegetation noise. part i: A prediction model, Acustica 85 (2) (1999) 228–240.

[3] O. Fegeant, Wind-induced vegetation noise. part ii: Field measurements, Acustica 85 (2) (1999) 241–249.

[4] S. Chen, S. Zhu, Y. Cai, An unsteady flow theory for vortex-induced vibration, Journal of Sound and Vibration 184 (1) (1995) 73–92.

[5] M. P. Païdoussis, S. J. Price, E. de Langre, Fluid-Structure Interactions: Cross-Flow-Induced Instabilities, Cambridge University Press, 2011.

[6] R. D. Blevins, Flow-induced Vibration, Van Nostrand Reinhold, 1990.

[7] O. Flachsbart, Messungen an ebenen und gewölbten Platten, in: Ergebnisse der Aerodynamischen Versuchsanstalt zu Göttingen - IV. Lieferung, Verlag von R. Oldenburg, München und Berlin, 1932, pp. 96–100.

[8] G. Bartoli, C. Mannini, A simplified approach to bridge deck flutter, Journal of Wind Engineering and Industrial Aerodynamics 96 (2) (2008) 229–256.

[9] T. Andrianne, G. Dimitriadis, Empirical modelling of the bifurcation behaviour of a bridge deck undergoing across-wind galloping, Journal of Wind Engineering and Industrial Aerodynamics 135 (2014) 129–135.

[10] M. Matsumoto, H. Shirato, T. Yagi, R. Shijo, A. Eguchi, H. Tamaki, Effects of aerodynamic interferences between heaving and torsional vibration of bridge decks: The case of Tacoma Narrows Bridge, Journal of Wind Engineering and Industrial Aerodynamics 91 (12-15) (2003) 1547–1557.

[11] Z. Q. Chen, M. G. Liu, X. G. Hua, T. M. Mou, Flutter, Galloping, and Vortex-Induced Vibrations of H-Section Hangers, Journal of Bridge Engineering 17 (3) (2012) 500–508.

[12] S. C. Luo, Y. T. Chew, T. S. Lee, M. G. Yazdani, Stability to translational galloping vibration of cylinders at different mean angles of attack, Journal of Sound and Vibration 215 (5) (1998) 1183–1194.

[13] Y. Nakamura, On the aerodynamic mechanism of torsional flutter of bluff structures, Journal of Sound and Vibration 67 (2) (1979) 163–177.

[14] J. S. Russell, On the Vibration of Suspension Bridges and other Structures; and the Means of preventing Injury from this Cause, in: Transactions of the Royal Scottish Society of Arts, 1841, pp. 304–314.

[15] G. G. Stokes, On the Effect of the Internal Friction of Fluids on the Motion of Pendulums, in: Mathematical and Physical Papers, Vol. 88, Cambridge University Press, Cambridge, 1912, pp. 1–10.

[16] Z. Lu, Q. Wen, X. He, Z. Wen, A flutter-based electromagnetic wind energy harvester: Theory and experiments, Applied Sciences (Switzerland) 9 (22) (2019).

[17] N. Wu, Y. He, J. Fu, P. Liao, Performance of a bistable flow-energy harvester based on vortex-induced vibration, Journal of Wind Engineering and Industrial Aerodynamics 217 (January) (2021) 104733.

[18] J. Allen, A. Smits, Energy harvesting eel, Journal of Fluids and Structures 15 (3-4) (2001) 629–640.

[19] S. Olivieri, G. Boccalero, A. Mazzino, C. Boragno, Fluttering conditions of an energy harvester for autonomous powering, Renewable Energy 105 (2017) 530–538.

[20] N. Chiereghin, D. J. Cleaver, I. Gursul, Unsteady lift and moment of a periodically plunging airfoil, AIAA Journal 57 (1) (2019) 208–222.

[21] A. Gayout, M. Bourgoin, N. Plihon, Rare Event-Triggered Transitions in Aerodynamic Bifurcation, Physical Review Letters 126 (10) (2021) 104501.

[22] S. Gao, L. Tao, X. Tian, J. Yang, Flow around an inclined circular disk, Journal of Fluid Mechanics 851 (2018) 687–714.

[23] Y. C. Fung, An Introduction to the Theory of Aeroelasticity, Dover Books on Aeronautical Engineering, Dover Publications, 2008.